IEEE Access
Multidisciplinary ⋮ Rapid Review ⋮ Open Access Journal

Received 14 June 2024, accepted 20 July 2024, date of publication 29 July 2024, date of current version 30 September 2024.

Digital Object Identifier 10.1109/ACCESS.2024.3435529

RESEARCH ARTICLE

Sensorless Speed Control of Induction Motor Drives Using Reinforcement Learning and Self-Tuning Simplified Fuzzy Logic Controller

QAZWAN ABDULLAH[1], (Senior Member, IEEE), NABIL FARAH[2], (Graduate Student Member, IEEE), MUSTAFA SAMI AHMED[3], (Student Member, IEEE), NOR SHAHIDA MOHD SHAH[4], (Senior Member, IEEE), ÖMER AYDOĞDU[5], (Member, IEEE), MD HAIRUL NIZAM TALIB[6], (Member, IEEE), YAHYA M. AL-MOLIKI[7], ABBAS UĞURENVER[8], MOHAMMED A. A. AL-MEKHALFI[9], MUHAMMAD ZAID AIHSAN[10], (Student Member, IEEE), AND ADEB SALH[11]

[1]Faculty of Electrical and Electronic Engineering, Universiti Tun Hussein Onn Malaysia, Parit Raja, Batu Pahat, Johor 86400, Malaysia
[2]Faculty of Engineering and Information Technology, University of Technology Sydney, Ultimo, NSW 2007, Australia
[3]Department of Communication Engineering, University of Technology-Iraq, Baghdad 84300, Iraq
[4]Faculty of Engineering Technology, University Tun Hussein Onn Malaysia, Pagoh, Johor 84600, Malaysia
[5]Faculty of Engineering and Natural Sciences, Konya Technical University, 42250 Konya, Türkiye
[6]Faculty of Electrical Engineering, Universiti Teknikal Malaysia Melaka, Melaka 76100, Malaysia
[7]Department of Applied Electrical Engineering, Al-Muzahimya Campus, College of Applied Engineering, King Saud University, Riyadh 11451, Saudi Arabia
[8]Faculty of Engineering, Electrical and Electronics Engineering Department, Istanbul Aydin University, 34295 Istanbul, Türkiye
[9]Department of Control and Mechatronics Engineering, Faculty of Electrical Engineering, Universiti Teknologi Malaysia, Skudai 81310, Malaysia
[10]Faculty of Electrical Engineering and Technology, University Malaysia Perlis (UniMAP), Arau, Perlis 02600, Malaysia
[11]Faculty of Information and Communication Technology, University Tunku Abdul Rahman, Kampar, Perak 31900, Malaysia

Corresponding authors: Nor Shahida Mohd Shah (shahida@uthm.edu.my) and Qazwan Abdullah (gazwan20062015@gmail.com)

This work was supported in part by King Saud University, Riyadh, Saudi Arabia, through the Researchers Supporting Project under Grant RSPD2024R1104. Communication of this research is made possible through monetary assistance by Universiti Tun Hussein Onn Malaysia (UTHM) and the UTHM Publisher's Office via Publication Fund E15216.

ABSTRACT Fuzzy logic controls (FLCs) have emerged as a promising solution for speed regulation in induction motor (IM) drives, offering adaptability to non-linearities, parameter variations, and external disturbances. However, conventional FLCs with fixed parameters and a huge number of rules can limit adaptiveness and increase system complexity, leading to deteriorated performance and high computational requirements. Moreover, reliance on costly encoders in traditional sensor-based IM drives introduces measurement errors and contributes toward the overall cost. To tackle these challenges, this paper proposes an integrated sensorless IM drive with a simplified self-tuning FLC (ST-FLC) and data-driven reinforcement learning (RL) for speed estimation. By employing a simplified 9-rule FLC instead of an intensive 49-rule counterpart and integrating a simple self-tuning mechanism based on mathematical equations, adaptiveness is maintained while computational overhead is reduced. Furthermore, the adoption of RL-based sensorless speed estimation eliminates reliance on encoder data, offering a cost-effective and computationally efficient alternative. Unlike conventional sensorless methods, the proposed sensorless-RL approach is data-driven and does not rely on motor parameters, leveraging a pre-trained policy for efficient speed estimation. Validation through simulation and experimentation on the dSPACE DS1104 platform demonstrates the efficacy of the proposed ST-FLC Sim 9-rule with sensorless RL. The method showcases accurate speed estimation, with

The associate editor coordinating the review of this manuscript and approving it for publication was Ton Duc Do.

simulation results comparable to standard 49-rule FLC and superior experimental performance. Significant computational time reduction is achieved with the proposed approach, resulting in a notable improvement in experimental performance metrics. Specifically, reductions of 50.5%, 20.4%, 15%, and 14.9% in settling time, current ripples, torque ripples, and current harmonics, respectively, underscore the practical benefits of the proposed integrated ST-FLC Sim 9-rule with sensorless-RL IM drive system.

INDEX TERMS FLC, ST-FLC, sensorless IM drives, RL, simplified rules, computation requirement.

NOMENCLATURE

AC	Actor-critic || alternating current.
DTC	Direct torque control.
DFOC	Direct field-oriented control.
DDPG	Deep deterministic policy gradient.
e/E	Speed error.
Δe	Change of speed error.
EKF	Extended kalman filter.
SMO	Sliding mode observer.
LSO	Luenberger State observer.
MRAS	Model reference adaptive system.
MF	Membership function.
EV	Electric vehicle.
FLC	Fuzzy logic control.
FOC	Field oriented control.
HCC	Hysteresis current control.
IM	Induction machine.
IFOC	Indirect FOC.
ST-FLC	Self-tuning FLC.
SF	Scaling factor.
NN	Neural network.
DNN	Deep neural network.
RL	Reinforcement learning.
MDP	Markov decision process.
PWM	Pulse width modulation.
VSI	Voltage Source Inverter.
Ψ_{rd}, Ψ_{rq}	Rotor flux of d- and q-axis.
v_{s}, v_{r}	Stator and rotor voltages.
v_{ds}, v_{qs}	d- and q-axis stator voltages.
v_{dr}, v_{qr}	d- and q-axis rotor voltages.
$\mathrm{i_s}$, $\mathrm{i_r}$	Stator and rotor currents.
i_{ds}, i_{qs}	d- and q-axis stator currents.
I^*_{qs}, I^*_{ds}	dq-axis stator reference currents.
i_{dr}, i_{qr}	d- and q-axis rotor currents.
I^*_α, I^*_β	α- and β-axis reference currents.
I_a, I_b, I_c	Three-phase stator currents.
I^*_a, I^*_b, I^*_c	Three-phase reference currents.
V_a, V_b, V_c	Three-phase stator voltages.
T_e	electrical torque.
T_L	Load torque.
ω	Machine speed.
ω_{est}	Estimated speed.
ω_{sl}	Slip frequency.
τ_{r}	Rotor time constant.
θ_{e}	Rotor flux position.
G_e	FLC input error SF.
G_{ce}	FLC input change of error SF.
G_{cu}	FLC output SF.
β	Self-tuning gain.
S	RL state space.
A	RL action space.
r	RL rewards.
π	RL policy.
γ	RL discount factor.

I. INTRODUCTION

Induction motors (IMs) are characterized by their simple construction, ruggedness, affordability, and low maintenance requirements. As such, IMs have been extensively utilized in a variety of industrial applications, including electric vehicles (EVs), oil and gas excavations, mills, and conveyors [1], [2]. To effectively utilize IMs in these applications, various control techniques (IM drives) are introduced, such as scalar, vector, and model predictive controls [3]. Vector control with torque and flux decoupling allows the IM to be controlled in a similar manner to separately excited DC motors, thus achieving satisfactory high performance with a fast-dynamic response, robust performance, and stable operations compared to the conventional V/F scalar controls [4], [5], [6]. Field Oriented Control (FOC) and Direct Torque Control (DTC) are the most commonly used vector control IM drives [7], [8], [9].

A vector control scheme consists of an outer speed control loop and an inner current/torque control loop. The primary function of these control loops is to generate switching pulses for the power electronic converter to effectively drive the motor [10]. In FOC, the switching pulses are generated using hysteresis current control (HCC) or other pulse width modulation (PWM) techniques such as sinusoidal PWM (SPWM) or space vector PWM (SVPWM). On the other hand, DTC directly generates the switching pulses based on a pre-defined switching table according to flux and torque errors. Both FOC and DTC have a fast-dynamic response and satisfactory state-state performance. However, DTC generates high steady-state torque ripples, variable switching frequency, and degrades performance at low-speed operations [11].

There are two types of FOC commonly used in IM drives, direct FOC (DFOC) and indirect FOC (IFOC). In DFOC, control variables are directly measured using sensors, which can be expensive to implement [12]. While IFOC indirectly anticipates the slip frequency by relying on the machine's dynamic model, thus IFOC does not require direct measurement of control variables, making it less sensitive to

parameter variations and ultimately reducing the cost of implementation [13]. Various researchers have implemented IFOC for IM drives and reported good and satisfactory performance [14], [15], [16], [17]. IFOC commonly employs HCC for switching pulse generation due to its simplicity, less currents and torque ripples, and reduced computational requirements compared to other PWM techniques [18], [19], [20].

The outer speed control loop is vital in any IM drive system, significantly affecting performance. For decades, Proportional Integral (PI) controller has been the main choice for IM drive speed regulation due to its simplicity and ability to offer faster dynamic response [21], [22]. However, PI controller with fixed gain values can experience various issues, including inability to cope with system non-linearities, parameter variations, and external disturbances [23], [24]. To overcome these issues, various adaptive speed controllers are introduced, such as employing a self-tuning PI controller [25] and other adaptive mechanisms [26], [27], [28]. Over the past 20 years, fuzzy logic controllers (FLCs) have been garnering significant attention as adaptive speed controllers for IM drives [10], [29], [30], [31]. FLCs excel with complex systems, adapt well to uncertain parameters, and are effective in precision-critical applications with varying conditions. Their adaptability and robustness enhance system performance and efficiency compared to traditional PI controllers [32], [33], [34].

FLC design comprises scaling factors (SFs), fuzzy rules and membership functions (MFs), which are selected based on expert knowledge and engineering skills [35], [36]. However, fixed SFs and a big number of fuzzy rules can degrade the drive performance and increase the computational requirement and/or hardware cost [37], [38]. Self-tuning FLCs (ST-FLCs) [13], [39], [40] and simplified rules-FLCs (SR-FLCs) [41], [42] have been introduced to maintain the adaptivity and reduce the computational burden of FLCs. In addition, a combination of self-tuning and simplified fuzzy has been introduced to enhance the adaptiveness and reduce computation requirements of FLCs simultaneously [43], [44]. However, the complexity of the self-tuning mechanism and/or using an additional FLC for self-tuning may degrade the performance and contribute to the overall system computational burden.

Speed control in IM drives is a closed-loop system that continuously compares the motor's actual speed to a desired reference speed in order to generate the desired control signal. Typically, the actual speed is measured through a speed sensor/ encoder. However, the encoder measurement is never accurate and varies depending on the encoder type and operating conditions. With more than $\mp 10\%$ offset of some encoders, high measurement errors are produced, affecting the accuracy of speed controller. Continuous measurement errors can result in accumulated steady-state ripples, significantly affecting the overall drive performance [45]. Sensorless speed controls have been introduced to eliminate the impacts associated with sensor measurement error and reduce the hardware cost [46].

Various sensorless techniques have been proposed in the literature to indirectly estimate the machine variables without sensing instruments [47], [48], [49]. Based on the motor mathematical model and measured variables (i.e., currents and voltages), reference and adaptive models can be developed (i.e., MRAS [34]) and used to indirectly estimate the motor speed. Other speed estimation techniques based on observers are common sensorless IM drives such as Extended Kalman Filter (EKF) [50], Luenberger state observer (LSO) [51], Sliding Mode Observer (SMO) [52], and Disturbance Observer [53]. However, MRAS highly depends on the motor model and parameters, which may not accurately represent the actual motor dynamics, and the parameters vary during operations. Additionally, MRAS can contribute toward the computation burden of the IM drive system. Thus, MRAS's less robustness to uncertainties and variations may result in inaccurate speed estimation, degrading the drive system performance [54]. In addition, observer-based techniques incorporate several parameters that require tuning and affect the speed estimation accuracy [55] and may require intensive online computation, contributing toward the computational burden of the overall IM drive system [56].

Machine learning-based approaches, including neural networks (NNs), have been utilized to overcome the related issues of MRAS and observers-based speed estimation methods. Several methods have been proposed to replace the adaptive and/or reference models of MRAS with NNs [57]. However, these methods normally train NNs based on offline pre-collected data, and the speed estimation highly depends on the amount and quality of training data. Additionally, gathering a large data set can be difficult and computationally intensive. If the trained NNs encounter conditions unseen in the training, undesired performance may occur [58], [59].

Recently, reinforcement learning (RL) based control methods have been employed to achieve various control tasks of the electrical machine drives, including RL-based speed, torque, and current controls [60], [61], [62]. RL allows online interaction with an environment (IM drive) through observation and rewards technique to learn a policy (controller) that can be used to replace the traditional controllers. The learned policy, when deployed, does not require online optimization, thus producing computationally efficient control compared to traditional control [63]. Recent studies have employed RL-based control techniques for sensorless speed estimation of electrical machine drives [64], [65], [66]. However, other methods were incorporated with RL, such as SMO and LSO observers, and traditional speed controllers were used. Thus, reducing the drive system's adaptiveness and increasing the computation requirements.

The common flaws of the various sensorless methods are inaccurate speed estimation at low-speed operations, ineffective load-disturbance rejection, the overall complexity of the drive, and high computation requirements and/or increased

hardware cost [67], [68], [69]. In addition, most existing sensorless IM drives utilize traditional fixed parameters speed controllers [70]. A few studies have combined sensorless techniques with adaptive speed controllers, including the use of FLCs or ST-FLCs [71], [72], [73], [74]. However, self-tuning complexity and big fuzzy rules remain issues that need to be addressed. In other words, an integrated sensorless IM drive that is adaptive, less complex, and computationally efficient has not been discussed in the literature.

This paper proposes a simple yet effective sensorless-RL for IFOC IM drive, which uses a self-tuning simplified rules FLC speed controller. The speed estimation is achieved through a pre-trained RL policy, eliminating encoder measurement errors. An RL agent interacts with the environment (IM drive) to receive observations, produce action, receive rewards, and modify its action until the desired rewards are achieved and optimal policy is obtained. This policy is learned offline through simulation; thus, no data collection is required, and the policy is computationally efficient since it does not require online optimization. To enhance adaptiveness, reduce complexity, and computational requirements of the speed controller, a simplified rules FLC with a self-tuning mechanism is employed. The number of fuzzy rules is reduced using a systemic rules simplification method [42], resulting in a computationally efficient IM drive system. The FLC fixed parameters are adaptively updated during operation using a simple mathematical equation self-tuning mechanism. The proposed method is an integrated IM drive system that accounts for various issues simultaneously. Unlike existing methods, the proposed method incorporates an accurate, less complex speed estimation along with an adaptive speed controller that accounts for adaptiveness and realization of the hardware implementation by using a self-tuning simplified rules FLC. The effectiveness of the proposed method is validated based on simulation and experimental results by conducting performance comparisons with sensor-based standard FLC speed control of IM drives, considering various speed operations and load conditions.

In summary, this article proposes an integrated, computationally efficient sensorless IM drive that incorporates:

i. ST-FLC Sim 9-rule is employed as the speed controller. The number of fuzzy rules is reduced to 9-rule using a systematic rules simplification method, resulting in a computationally efficient controller. The FLC parameters are adaptively updated during operation using a simple mathematical equation self-tuning mechanism, enhancing the controller's adaptiveness.
ii. Speed estimation is achieved through a pre-trained RL policy, eliminating the need for an encoder and associated measurement errors. The RL agent interacts with the IM drive environment, receiving observations, producing actions, and receiving rewards to learn the optimal policy offline through simulation. The pre-trained RL policy is computationally efficient since it does not require online optimization.
iii. The proposed method is an integrated IM drive system that simultaneously addresses various issues, such as accurate speed estimation, adaptive speed control, and computational efficiency. It incorporates an accurate, less complex speed estimation along with an adaptive speed controller that accounts for adaptiveness and hardware implementation using ST-FLC Sim 9-rule.

The rest of the paper is organized as follows: Section I presents the mathematical model of the induction motor, as well as the structure and principle of (IFOC). Section II discusses speed control methods, including standard FLC, ST-FLC and fuzzy rules simplification. Section III discusses the proposed sensorless-RL control method. Sections IV and V present the simulation, experimental results, and analysis and comparison of the proposed method with standard FLC. Finally, Section VI summarises the paper's content and highlights the key findings.

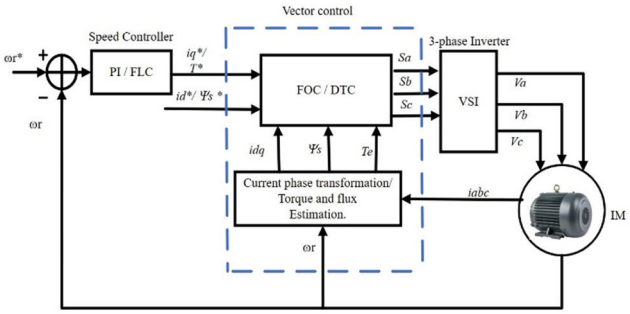

FIGURE 1. General block diagram of IM drive.

II. DYNAMIC MODELING OF IM DRIVES

The typical IM drive system comprises several essential components, including a speed controller, a vector control scheme (FOC or DTC), a three-phase inverter, and an electric motor. Depending on the chosen vector control method, PWM switching pulses are generated to regulate the output voltages of the inverter, which, in turn, controls the motor's operation.

Current sensors and a speed encoder are utilized to measure motor currents and speed, which are fed back to the controller. The speed controller and, where applicable, inner current or torque controllers (depending on the vector control method employed) compare the measured signals with reference signals. A general IM drive system is depicted in the block diagram shown in Fig.1.

A. MATHEMATICAL MODEL OF IM

To design a controller for a physical system, the equations governing that system must be represented mathematically, which is known as a system mathematical model. For efficient IM drive performance, creating a precise mathematical model is crucial. The accuracy and effectiveness of vector control and sensorless techniques in IM drives depend heavily on the accuracy of the motor model used. With the help of a phasor diagram and phase transformation, the three-phase (Fig.2 (a)) can be represented by an equivalent two-phase IM

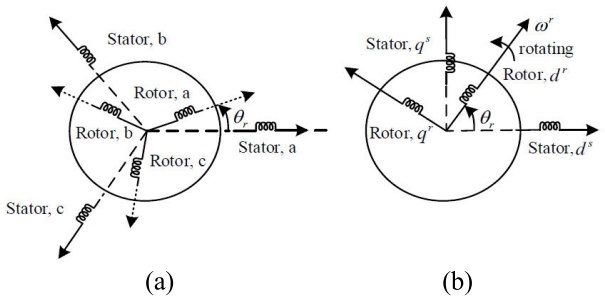

FIGURE 2. IM phasor representation in (a) three-phase, and (b) two-phase equivalent.

machine with two axes, d-axis and q-axis (Fig.2 (b)). In a synchronous reference, the voltage equations are expressed in (1), as shown at the bottom of the next page, where V_{qs}, V_{ds}, V_{qr}, V_{dr} are the applied d-axis and q-axis voltages to the stator and rotor; and i_{qs}, i_{ds}, i_{qr}, i_{dr} are the corresponding d-axis and q-axis stator current and rotor currents. R_s, R_r are the stator and rotor resistances .L_s, L_r denotes stator and rotor inductances respectively, whereas L_m is the mutual inductance. ω_s, synchronous speed, ω_r,rotor speed and, ρ, the Laplace operator.

In state space form, the stator and rotor currents (i_s, i_r) are used as state variables and can be expressed as follows:

$$\frac{d}{dt}\begin{bmatrix} i_s \\ i_r \end{bmatrix} = \frac{1}{\sigma L_s L_r}\begin{bmatrix} -R_s L_r - j\omega_m L_m^2 & R_r L_m - j\omega_m L_m L_r \\ R_s L_m + j\omega_m L_m L_s & -R_r L_s + j\omega_m L_s L_r \end{bmatrix}\begin{bmatrix} i_s \\ i_r \end{bmatrix} + \frac{1}{\sigma L_s L_r}\begin{bmatrix} L_r & -L_m \\ -L_m & L_r \end{bmatrix}\begin{bmatrix} v_s \\ v_r \end{bmatrix} \quad (2)$$

where σ is sigma and equal to $\sigma = 1 - \frac{L_m^2}{L_s L_r}$.

The electrical torque of IM can be described by the interaction between the rotor flux and stator currents. By resolving the variable into dq components, the electrical torque is expressed in (3). Meanwhile, the mechanical torque depends on the mechanical load applied to the motor shaft as well as the inertia and friction of the motor, and the rotor speed, which can be expressed as in (4).

$$T_e = \frac{3}{2} P L_m \left(i_{qs} i_{dr} - i_{ds} i_{qr}\right) \quad (3)$$

$$T_e - T_L = J\frac{d\omega_r}{dt} + B\omega_r \quad (4)$$

where P, T_L, J and B denote respectively the number of poles, external load, inertia and friction of the induction motor respectively.

B. INDIRECT FIELD ORIENTED CONTROL (IFOC)

The FOC imitates the concept of separately excited dc motor drive where the torque and the flux are controlled by two independent orthogonal variables known as the armature and field currents. In FOC, there are two control inputs, the torque component, represented by the q-axis, and the flux component, represented by the d-axis. By representing the IM model in a rotating synchronous reference frame, the torque component represented by i_{qs} and flux component represented by i_{ds}. Hence, the voltage equations are expressed as follows:

$$\frac{d\Psi_{rd}}{dt} = -\frac{1}{\tau_r}\Psi_{rd} + (\omega_s - \omega_r)\Psi_{rq} + \frac{L_m}{\tau_r} I_{sd} \quad (5)$$

$$\frac{d\Psi_{rq}}{dt} = -\frac{1}{\tau_r}\Psi_{rq} - (\omega_s - \omega_r)\Psi_{rd} + \frac{L_m}{\tau_r} I_{sq} \quad (6)$$

where Ψ_{rd} and Ψ_{rq} represent the d-and q-axis rotor flux respectively, assuming $\Psi_{rd} = \Psi_r$ and $\Psi_{rq} = 0$.

When the rotor flux is locked to the d-axis, the following new expression is obtained:

$$\Psi_r = \frac{L_m}{\tau_r s + 1} I_{sd} \quad (7)$$

$$(\omega_s - \omega_r) = \omega_{sl} = \frac{L_m}{\tau_r}\frac{I_{sq}}{\Psi_r} \quad (8)$$

where $\tau_r = \frac{L_r}{R_r}$ rotor is time constant. According to (7), the rotor flux value Ψ_r is driven by stator flux direct axis current I_{sd}. The electrical torque of the motor can be illustrated by the interface between the rotor flux and I_q current as expressed in the following equation:

$$T_e = \frac{3}{2}\frac{P}{2}\frac{L_m^2}{L_r}\Psi_{rd} I_{sq} \quad (9)$$

The slip frequency, ω_{sl} depends on the quadrature axis of the stator current I_{sq}. The rotor flux Ψ_{rd} depends on the d-axis current, and can be considered as a constant value in a steady state condition. Thus, the electrical torque in (9) can be simply controlled by controlling the q- axis stator current, I_{sq}.

The rotor flux position, θ_e for coordinate transform is generated from the integration of rotor speed, ω_r and slip frequency, ω_{sl} as follow:

$$\theta_e = \int \omega_r + \omega_{sl} \quad (10)$$

Equation (10) is used to estimate the position of the rotor flux in IFOC methods indicated as theta calculation in Fig.3.

In IFOC based on IM drive system, as shown in Fig. 3, the reference flux current I_{ds}^* is constant. The measured speed of the motor ω_r is compared with a reference speed ω_r^*. The comparison produces an error that becomes an input for the speed controller. The output of the speed controller is the q-axis current reference component I_{qs}^*. The I_{qs}^* and I_{ds}^* d-q rotating frame is converted into two orthogonal stationary frames (I_α^*, I_β^*) by using inverse park transformation with the help of a theta. Then, two-phase stationary frame quantities (I_α^*, I_β^*) are transformed into three-phase reference quantities (I_a^*, I_b^*, I_c^*) by using inverse Clark transformation. The three-phase reference currents are compared with the three-phase stator currents (I_a, I_b, I_c) using hysteresis current controller. The comparison produces switching signals to control the three-phase Voltage Source Inverter (VSI). Three-phase voltages (V_a, V_b, V_c) are produced to drive the IM at any demand speed.

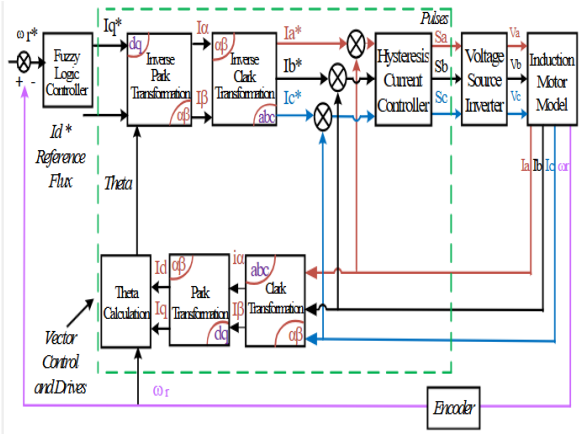

FIGURE 3. Sensor-based IFOC of IM drive.

III. SPEED CONTROLLER

Speed controller plays a significant role in the overall drive system performance effectiveness. FLCs enhance the speed control adaptiveness and outperform traditional controllers in systems with varying conditions. Yet, standard FLCs with fixed SFs and a large number of rules can still limit the drive performance and contribute to a huge computational burden on the system. This section discusses the design of standard FLC, fuzzy rules simplification and self-tuning mechanism.

A. STANDARD FLC

FLC is an intelligent controller that has proven to be effective in controlling the speed of induction motors. The FLC's basic structure comprises three stages: fuzzification, rule-base, and defuzzification. Fuzzification involves mapping the crisp inputs into fuzzy sets, rule-base is where the fuzzy logic rules are defined, and defuzzification converts the fuzzy output into crisp control signals. The FLC has demonstrated good performance in various IM drive systems and is a popular choice for controlling motor speed. For FLC speed controller, two crisp inputs are considered, speed error and change of error (e, Δe), and one output (Δu).

The FLC operation involves converting the crisp input variables to a fuzzy variable (fuzzification), calculating the fuzzy output based on designed rules (rule-base), and converting the fuzzy output variable to a crisp output variable (defuzzification). The design of FLC includes selecting MFs, designing fuzzy rules and selecting SFs. Various types of MFs can be used, such as triangular, trapezoidal, Gaussian, and sigmoidal. In this research, triangular and trapezoidal MFs have been chosen due to their less computational requirement compared to other types of MFs. The use of these MFs reduces the processing time and computational cost of the FLC, making it more efficient for real-time applications [75].

The number of MFs can be selected depending on the knowledge of system operations. However, for AC motor speed control, there are three standard MF numbers that have been validated to work effectively, (3 × 3), (5 × 5), and (7 × 7) equally distributed MF numbers. Bigger numbers and /or unequally distributed MFs may be specifically designed for a certain type of machine based on the designer's knowledge and experience [37]. In this research, 7 × 7 MFs are considered, as shown in Fig.4.

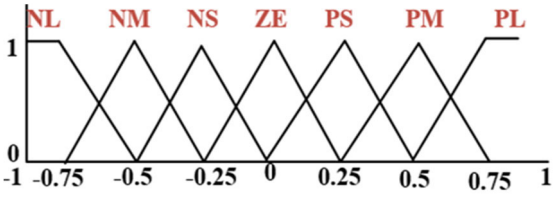

FIGURE 4. Standard FLC 7 × 7 MFs.

The number of MFs in standard FLC determines the number of fuzzy rules; for instance, (3 × 3), (5 × 5), and (7 × 7) MFs produce 9,25, and 49 fuzzy rules [42]. With the standard (7 × 7) MFs (Fig.4), the rule base of (49) can be designed accordingly [76]. Based on the IF-THEN principle, these rule bases generate fuzzy output. FLC (MFs) are typically represented as NL, NM, NS, ZE, PS, PM, and PL, corresponding to negative large, negative medium, negative small, zero, positive small, positive medium, and positive large, respectively. With two fuzzy inputs, speed error and change of speed error (e, Δe), and one output (Δu), the 49 fuzzy rules are designed as presented in Table 1.

TABLE 1. FLC rule-base of 7 × 7 MFS.

E / ΔE	NL	NM	NS	ZE	PS	PM	PL
PL	**ZE**	PS	**PS**	**PL**	**PL**	PL	**PL**
PM	**NS**	ZE	**PS**	**PM**	**PL**	PL	**PL**
PS	**NS**	NS	**ZE**	**PS**	**PS**	PL	**PL**
ZE	**NL**	NM	**NS**	**ZE**	**PS**	PM	**PL**
NS	**NL**	NL	**NS**	**NS**	**ZE**	PS	**PS**
NM	**NL**	NL	**NL**	**NM**	**NS**	ZE	**PS**
NL	**NL**	NL	**NL**	**NL**	**NS**	NS	**ZE**

For faster convergence of FLC, the MFs range is normalized in the range [−1,1] to cover forward (positive) and reverse (negative) speed operations. However, the fuzzy input speed error (e) can be in the range [−1400,1400] rpm. Thus, SFs are required to normalize the fuzzy inputs and output to the desired range suitable for MFs coverage. In FLC

$$\begin{bmatrix} V_{qs} \\ V_{ds} \\ V_{qr} \\ V_{dr} \end{bmatrix} = \begin{bmatrix} R_s+\rho L_s & L_s\omega_s & \rho L_m & L_m\omega_s \\ -L_s\omega_s & R_s+\rho L_s & -L_m\omega_s & \rho L_m \\ \rho L_m & L_m(\omega_r-\omega_s) & R_r+\rho L_r & L_r(\omega_r-\omega_s) \\ -L_m(\omega_s-\omega_r) & \rho L_m & -L_r(\omega_s-\omega_r) & R_r+\rho L_r \end{bmatrix} \begin{bmatrix} i_{qs} \\ i_{ds} \\ i_{qr} \\ i_{dr} \end{bmatrix} \quad (1)$$

speed controller, three SFs are used, namely error SF (G_e), change of error SF (G_{ce}), and output SF (G_{cu}). The values of these SFs typically in standard FLC are determined based on a trial-and-error process. The overall FLC speed controller architecture is depicted in Fig.5.

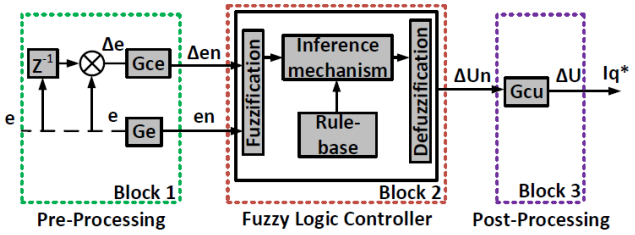

FIGURE 5. Standard FLC architecture.

B. FUZZY-RULE SIMPLIFICATION

FLC rule-base design essentially depends on engineering knowledge and experienced operation of the controlled system [77]. Based on [42], the fuzzy control rules of IM drives or any similar second order system can be determined from the general dynamic step response of the system. From the system step response, the system behavior aspects can be anticipated, and the phase plane trajectory can be mapped as shown in Fig.6. The rule-base table can be formed from the area and points of the phase plane which includes all possible step responses.

In trajectory mapping of the step response of the system (Fig.7 (b)), the route of the rules starts from the outer area of the phase plane and continuously moves toward the equilibrium point, where the error (E) and change of error (ΔE) are zero. The rules route usually passes through all step response areas (A1-A4), two cross-over points (b1, b2), and two peak-valley points (c1, c2), which creates a longer rules route. However, as the rules take a shorter route to the equilibrium point, system stability increases. Shortening the rules route reduces the number of rules required. The 49 rules of (7 × 7) MFs can be reduced by selecting only the rules that form the shortest route to the equilibrium point. Nine rules out of 49 create a short route to the equilibrium point, where the error (E) and change of error (ΔE) are zero. The simplified 9 rules are presented in Table 2, where the selected rules are highlighted. The FLC of (7 × 7) MFs has a very high output accuracy, but it utilizes 49 rules that increase the online computation of the fuzzy system and/or the hardware cost. In this simplified rule method, only 9 rules are considered, while the remaining 40 rules are deleted. This reduces the computation capabilities required by the fuzzy system. Thus, system hardware can be constructed with a high output accuracy of FLC and without requiring additional processing capabilities.

C. SELF-TUNING MECHANISM

In standard FLC, error SF (G_e), change of error SF (G_{ce}), and output SF (G_{cu}) are determined based on trial-and-error, which is time-consuming and reduces FLC adaptiveness to

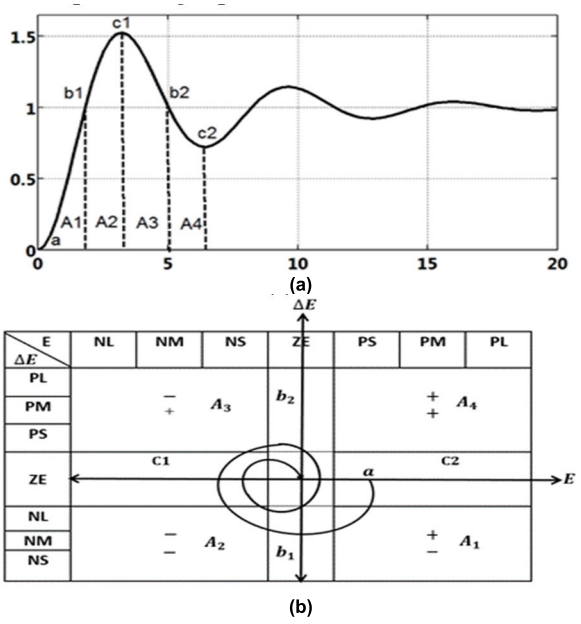

FIGURE 6. (a) Dynamic behaviour of step response for second order system, (b) Phase-plane trajectory mapping.

changes in operating conditions. The error SF (G_e), change of error SF (G_{ce}) can be computed based on the maximum speed and maximum torque per ampere of the machine, as shown in [37], [41]. However, the output SF (G_{cu}) cannot be computed directly and has a significant impact on the performance compared to input SFs [38], [40]. Thus, it is very essential to develop a self-tuning mechanism to adaptively update the value of G_{cu} online during operation. In this research, a simple technique is employed to tune the output SF based on the relationship between the FLC input (e) and FLC output ((Δu). Based on the obtained simplified rules, the condition of FLC input (change of error) has less impact on FLC output. Therefore, the relationship between FLC input speed error (e) and FLC output ((Δu) can be summarized into the following:

i. When the speed error is very big positive or negative (transient start-up), higher gain multiplication for the output ((Δu) is required to ensure faster rise time.
ii. When speed error is positive small or negative, lower gain multiplication for the output ((Δu) is required to ensure faster settling time and lower overshoot.
iii. When the speed error is zero (steady state), medium gain multiplication for the output ((Δu) is required to prevent oscillation due to lower or zero gain.

Based on these relationships, a gain multiplication, β, can be used to tune the FLC output SF. The gain β can be expressed based on FLC input of speed error (e) as follows

$$\beta = \left(\frac{1}{M} + |e|\right) K \tag{11}$$

The variable β is the non-linear gain online updating factor for the output scaling factor (G_{cu}). It is formulated based on the relationship between FLC input speed error (e) and FLC

output ((Δu). For instance, if the value of, e, is small, then , G_{cu}, need to be reduced, and if, e, is big, then, G_{cu}, need to be increased. Hence, the β value is formulated based on this concept by adding, $|e|$, to the fraction ($\frac{1}{M}$) to avoid lower gain multiplication (βG_{cu}) when, e, is very small. The value of M is chosen based on the number of uniform input fuzzy partitions (number of MFs), which is 7 in our case. The value of K is chosen to make the possible variation in β, which is set to 1.3 based on the tuning process. The proposed ST-FLC mechanism shown in Fig.7 utilizes a simple mathematical algorithm to adaptively update the output SF based on the input speed error. This can enhance the adaptiveness of FLC with no additional computational requirement.

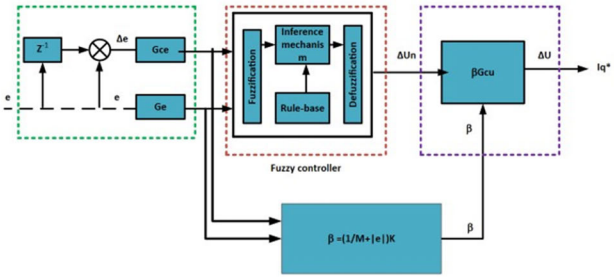

FIGURE 7. Self-tuning mechanism.

TABLE 2. Simplified 9 rule-base of 7 × 7 MFS.

E / ΔE	NL	NM	NS	ZE	PS	PM	PL
PL	ZE	PS	PS	PL	PL	PL	PL
PM	NS	ZE	PS	PM	PL	PL	PL
PS	NS	NS	ZE	PS	PS	PL	PL
ZE	NL	NM	NS	ZE	PS	PM	PL
NS	NL	NL	NS	NS	ZE	PS	PS
NM	NL	NL	NL	NM	NS	ZE	PS
NL	NL	NL	NL	NL	NS	NS	ZE

* Simplified rules:

1. $IF\{E\ is\ NL\ and\ \Delta E\ is\ ZE\}THEN\ \Delta U\ is\ NL$
2. $IF\{E\ is\ NM\ and\ \Delta E\ is\ ZE\}THEN\ \Delta U\ is\ NM$
3. $IF\{E\ is\ NS\ and\ \Delta E\ is\ ZE\}THEN\ \Delta U\ is\ NS$
4. $IF\{E\ is\ ZE\ and\ \Delta E\ is\ PS\}THEN\ \Delta U\ is\ PS$
5. $IF\{E\ is\ ZE\ and\ \Delta E\ is\ ZE\}THEN\ \Delta U\ is\ ZE$
6. $IF\{E\ is\ ZE\ and\ \Delta E\ is\ NS\}THEN\ \Delta U\ is\ NS$
7. $IF\{E\ is\ PS\ and\ \Delta E\ is\ ZE\}THEN\ \Delta U\ is\ PS$
8. $IF\{E\ is\ PM\ and\ \Delta E\ is\ ZE\}THEN\ \Delta U\ is\ PM$
9. $IF\{E\ is\ PL\ and\ \Delta E\ is\ ZE\}THEN\ \Delta U\ is\ PL$

IV. SENSORLESS-RL BASED SPEED ESTIMATION

Sensorless techniques for machine drives are gaining attention across both research and industrial sectors due to their capacity to estimate machine variables indirectly without the need for sensing instruments. However, existing sensorless methods face challenges such as inaccurate estimation during low and zero-speed operations, system instability, and complexity. These limitations have prompted the exploration of alternative approaches, including speed estimation methods that leverage motor mathematical models and measured variables (currents and voltages) to estimate motor speed indirectly, such as MRAS and observer-based methods. While these techniques eliminate the use of sensor, they are susceptible to inaccuracies due to varying motor parameters and computational burdens.

To address these issues, machine learning-based approaches, notably neural networks (NN), have been employed to enhance speed estimation methods. However, these approaches often rely on offline pre-collected data for training, leading to challenges in acquiring sufficient and representative datasets. In contrast, this paper proposes a Reinforcement Learning (RL) based sensorless approach for IM drive speed estimation. RL facilitates online interaction with the environment, allowing the learning of a policy to estimate motor speed without the need for extensive data collection. Here, a deep deterministic policy gradient (DDPG) agent, a model-free, online, off-policy RL is used.

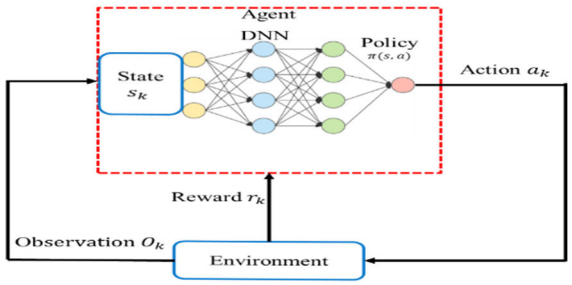

FIGURE 8. RL learning diagram.

The 49 rules of (7 × 7) MFs can be reduced by selecting only the rules that form the shortest route to the equilibrium point. Nine rules out of 49 create a short route to the equilibrium point, where the error (E) and change of error (ΔE) are zero. The simplified 9 rules are presented in Table 2, where the selected rules are highlighted. The FLC of (7 × 7) MFs has a very high output accuracy, but it utilizes 49 rules that increase the online computation of the fuzzy system and/or the hardware cost. In this simplified rule method, only 9 rules are considered, while the remaining 40 rules are deleted. This reduces the computation capabilities required by the fuzzy system. Thus, system hardware can be constructed with a high output accuracy of FLC and without requiring additional processing capabilities.

RL methods are categorized into value-based and policy-based algorithms. The value-based methods learn the Q-function that estimates the Q-value of state-action pairs $(s, a) \in S \times A$. Policy gradient methods directly learn the parameterized policy based on feedback from the environment. The actor-critic (AC) structure is common in policy gradient RL methods, with two ANN models that optionally share parameters: i) Critic updates the parameters of value functions; ii) Actor updates the policy parameters under the guidance of the critic. Under the AC structure, policy function can be either stochastic or deterministic. The stochastic policy is modelled as a probability distribution: $a \sim \pi_\theta(a|s)$, while the deterministic policy is modelled as a deterministic decision: $a = \pi_\theta(s)$.

The deterministic policy gradient (DPG) method first used deterministic policy [77]. Then, the deep deterministic policy

TABLE 3. Training and DDPG hyper parameters.

Parameter	Value
Critic learning rate	2.5×10^{-4}
Critic gradient threshold	1
Critic Regularization Factor	2.5×10^{-4}
Discount Factor	0.99
Experience Buffer Length	2×10^{6}
Mini Batch Size	64
Target Smooth Factor	0.005
Target Update Frequency	2
Clustering DNN learning rate	5×10^{-3}

gradient (DDPG) was developed by combining the DPG and DQN [38]. The DDPG extends the discrete action space of the DQN to continuous space while learning a deterministic policy. The gradient of deterministic policy $a = \pi_\theta(s)$ is expressed as:

$$\nabla J(\theta) = \mathbb{E}_s \sim \mu_\theta \left[\nabla_a Q_{\pi_\theta}(s, a) \mid_{a=\pi_\theta(s)} \nabla_\theta \nabla_\theta(s) \right] \quad (12)$$

where $J(\theta)$ represents the objective function that the agent is trying to maximize, θ symbolizes the parameters of the policy, denoted as $\pi_\theta(s)$. μ_θ represents the distribution of states s under the policy $\pi_\theta(s)$, and the expectation $E_s \sim \mu_\theta$, is taken over this distribution. $Q_{\pi_\theta}(s, a)$ is the action-value function, representing the expected cumulative reward of taking action a in state s under the policy $\pi_\theta(s)$.$\nabla_a Q_{\pi_\theta}(s, a) \mid_{a=\pi_\theta(s)}$ the gradient of the action-value function with respect to the action, evaluated at the action chosen by the policy, and $\nabla_\theta \nabla_\theta(s)$ the gradient of the policy with respect to its parameters.

The selection of appropriate observations, rewards and action is very crucial to ensure effective training of RL and obtain optimum policy. For speed estimation of IM drives, standard observations are measured dq currents, measured dq voltages, estimated speed at a previous time step, ω_{est}^{k-1}, and reference speed which can be expressed as:

$$o^k = \left[\omega^*, \omega_{est}^{k-1}, i_d^k, i_q^k, v_d^k, v_q^k \right]^T \quad (13)$$

The error between estimated and reference speed, along with a penalty term are set as reward function as follows:

$$r^k = -\left(w_1 e_\omega^k + w_2 P^k \right) \quad (14)$$

where w_1 and w_2 are the reward gains; P^k is a penalty term to ensure safe operation and discourage the agent from high-speed and/or overcurrent region by penalizing the agent if the estimated speed ω_{est}^k or measured current exceeds the maximum values.

The overall block diagram of sensorless IM drives with sensorless-RL is illustrated in Fig. 9. Similar to the MRAC speed estimation, the inputs for the sensorless-RL algorithm consist of the observed currents and voltages. However, in sensorless-RL, the parameter-dependent MRAC models are substituted with a computationally efficient RL policy. This policy is trained and reinforced through rewards to effectively map actions. The training process involves a maximum of 4000 episodes, each comprising sufficient trajectories (time steps) for the agent to grasp the dynamics associated with it. The termination condition for training is based on the average rewards obtained, which is set to a value of -50 to ensure sufficient training episodes and convergence of the episode reward to the long-term reward.

During the 4000 episodes, the DDPG agent aims to maximize cumulative episode rewards by avoiding low-reward actions until both cumulative and average rewards stabilize at lower values, as shown in Fig. 11. The training and DDPG RL hyperparameters utilized are detailed in Table 3. Finally, the trained RL policy is deployed and tested at different operating conditions, which will be discussed in the next section.

TABLE 4. Quantitative comparison of standard FLC 49-rule and the proposed ST-FLC sim 9-rule with/without sensorless sensorless-RL.

Property		T_s(s)	OS%	ω_{ripple} (rpm)	$i_{a_{ripple}}$ (A)	T_{ripple} (Nm)
Controller	Speed acquisition					
Standard FLC 49-rule.	Sensored	0.1173	0.3952	0.1389	0.8514	2.1732
	sensorless	0.1164	0.625	0.2847	0.8374	2.1945
ST-FLC Sim 9-rule	Sensored	0.1183	0.5349	0.1457	0.8579	2.1097
	sensorless	0.1176	0.3895	0.2595	0.8426	2.1925

V. SIMULATION RESULTS

The performance of the proposed ST-FLC sensorless-RL of IM drives is validated through numerical simulation in MATLAB/SIMULINK based on 1.5 kW IM with parameters presented in Table 5 (appendix). To show the effectiveness of the proposed method, performance comparisons are conducted with the conventional control method.

The standard 49-rule FLC speed controller is compared with the proposed ST-FLC simplified 9-rule with/without sensorless-RL speed estimation at different operating conditions. The performance of rotor speed, ω_r, stator phase A current, $i_{a,}$ and torque, T_e are captured at rated speed 1400 rpm, 700 rpm, 300 rpm and 100 rpm as shown in Figs. 12 and 13. In addition, both control schemes are tested against load disturbance by applying 10 Nm load torque at 1s during forward operation and 3.5s during reverse operation, as depicted in Fig.14.

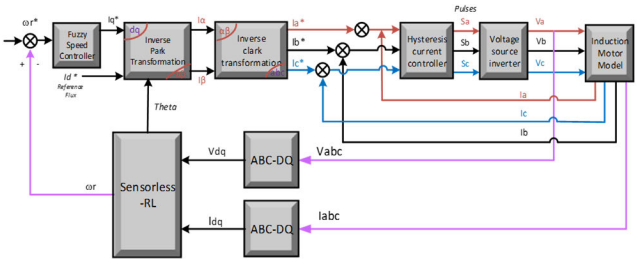

FIGURE 9. Overall block diagram of the proposed sensorless-RL self-tuning simplified rules FLC of IM drives.

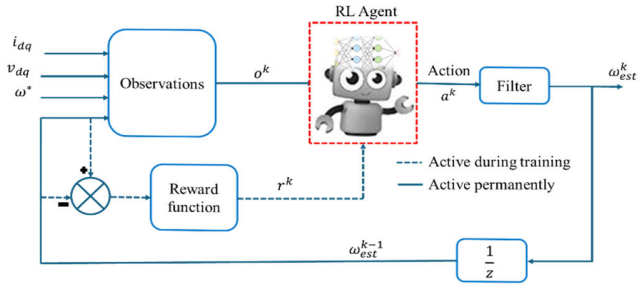

FIGURE 10. Proposed sensorless-RL speed estimation.

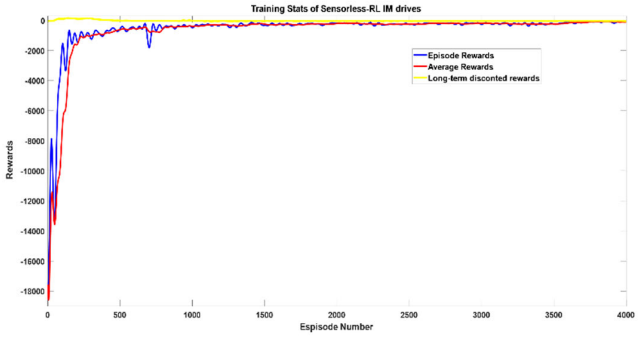

FIGURE 11. Training states of sensorless-RL.

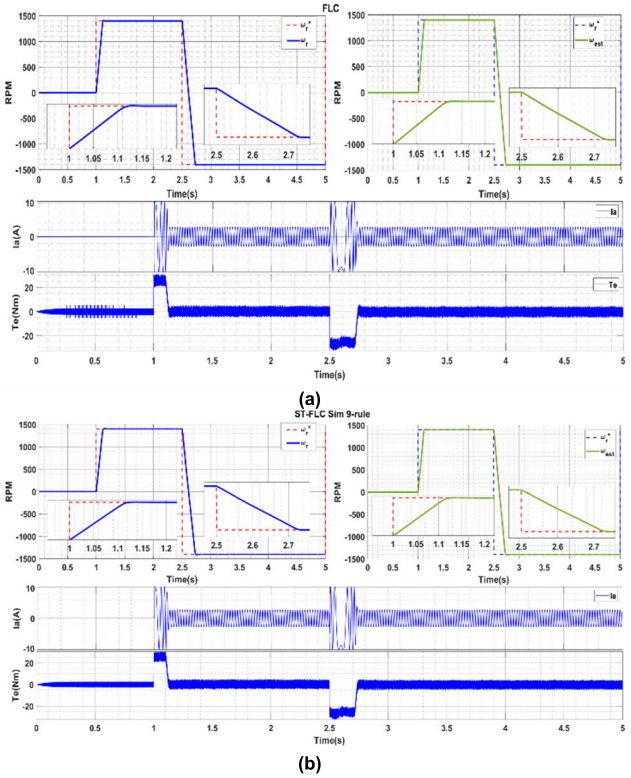

FIGURE 12. Performances of speed and current with and without sensorless-RL speed estimation for (a) 49-rule FLC and (b) ST-FLC Sim 9-rule.

The comparison results show that the proposed ST-FLC Sim 9-rule, with and without sensorless-RL speed estimation, performs effectively. The ST-FLC Sim 9-rule maintains performance comparable to the standard 49-rule FLC across different speeds and load conditions. The estimated speed accurately tracks the desired reference speed, even at low speeds (100 rpm), demonstrating the effectiveness of the proposed sensorless-RL method in estimating motor speed.

Typically, FLC with a big number of rules (49-rule) can perform better than a small number of rules (9-rule) during simulation evaluation since the computation effect is not an issue. However, with the help of the self-tuning mechanism, the proposed ST-FLC Sim 9-rule has shown comparable performance to the standard FLC 49-rule. To get a deeper insight into the performance comparison, quantitative analysis is conducted by computing some transient and steady-state performance characteristics. The property of settling time (T_s), Overshoot ($OS\%$), and speed, current and torque steady-state ripples are computed for the standard and proposed controller with both sensored and sensorless-RL speed estimation.

At start-up speed from 0 to 1400 rpm, T_s and $OS\%$ are obtained. The speed, current and torque steady-state ripples are computed for 0.5s (N =10000) of steady-state signals at 1400 rpm with 2 Nm. generally, a steady-state ripple of a signal can be computed based on the following:

$$x_{ripple} = \sqrt{\frac{1}{N}\sum_{i=1}^{N}(x_i^* - x_i)^2} \tag{15}$$

where N is the number of samples, x_i^* and x_i are the reference and actual signals which can be the speed, current and torque signals.

The resultant quantitative comparison between the standard and the proposed method with both sensored and sensorless-RL speed acquisition is presented in Table 4. Both controllers maintain fast settling time (T_s) and low overshoot (OS%) for the drive system. The proposed method with sensorless-RL demonstrates better transient results than the sensored method. Additionally, both the standard and proposed methods exhibit slightly higher speed ripples with sensorless-RL. However, the torque and current ripples are approximately the same or better than those in sensor-based IM drives. The higher speed ripples in sensorless-RL compared to sensor-based IM drives are due to the absence of sensor measurement errors in the simulation, as the measurements are considered ideal.

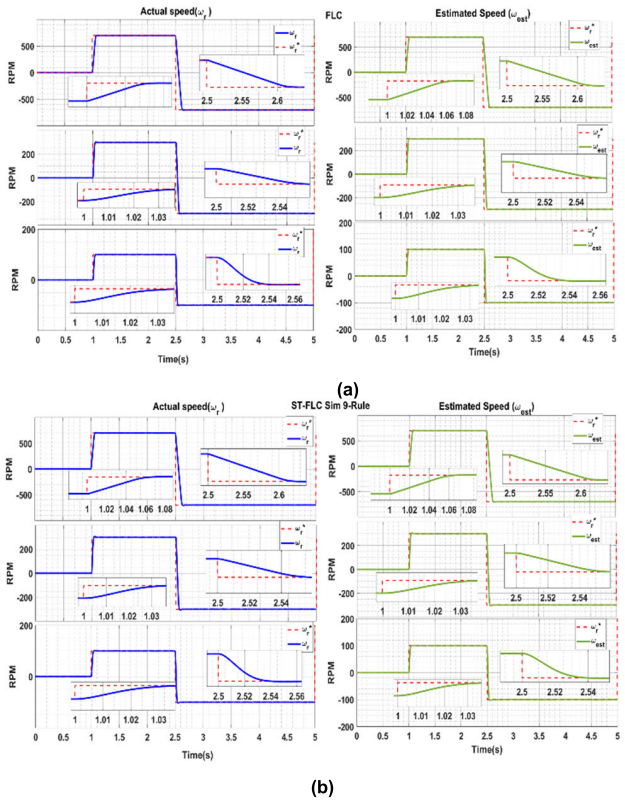

FIGURE 13. Performances with and without sensorless-RL speed estimation at different speed operation, 700rpm, 300rpm and 100rpm for, (a) 49-rule FLC, and (b) ST-FLC Sim 9-rule.

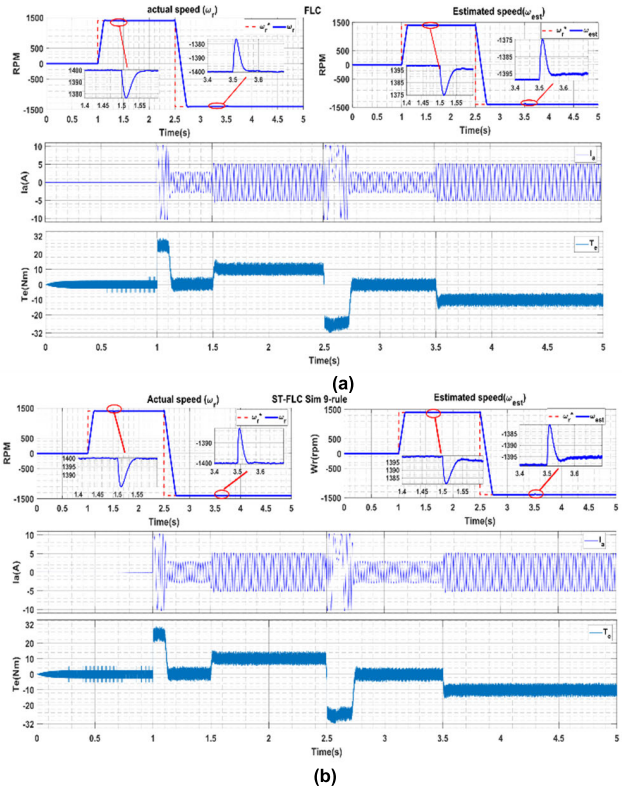

FIGURE 14. The load disturbance comparisons with and without sensorless-RL speed estimation at 1400rpm and 10Nm for, (a) 49-rule FLC, and (b) ST-FLC Sim 9-rule.

VI. EXPERIMENTAL RESULTS

To verify the simulation results and effectiveness of the proposed ST-FLC Sim 9-rule-based sensorless-RL IM drives, experimental validation is conducted based on 2 HP IM and dSPACE DS 1104 control board. The overall experimental setup shown in Fig.15 incorporates dSPACE DS 1104, gate drive, three phase inverter and PC. The control algorithm is implemented in MATLAB/SIMULINK and loaded as C-code into the DS 1104 board. The dSPACE receives sensor feedback signals and processes them to generate switching pulses and send them to the gate drives. The three-phase output voltages of the inverter are connected to the motor to operate accordingly. Additionally, the DC input voltage (537.3 V) to the inverter is generated through a three-phase rectifier and capacitor filter.

The first performance test evaluates the effectiveness of the proposed sensorless RL for speed estimation compared to speed encoder measurements. The ST-FLC Sim 9-rule speed control is used in both tests. The comparison between estimated and measured speeds at 1400 rpm, 1000 rpm, 500 rpm, and 100 rpm are shown in Fig. 16. The sensorless-RL may experience slow settling when it approaches the desired speed due to the limitations and penalties designed during training to prevent the RL agent from exceeding the rated speed. As a result, the estimated speed quickly aligns with the measured speed but slows down as it gets close to the desired speed to ensure it does not exceed the rated speed. The proposed sensorless-RL has demonstrated accurate speed estimation across various speeds, including a low speed of 100 rpm.

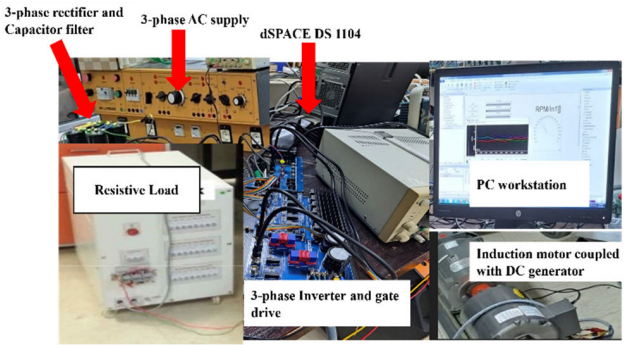

FIGURE 15. IM drive experimental setup.

TABLE 5. Training and DDPG hyperparameters.

Parameter	Value
Critic learning rate	2.5×10^{-4}
Critic gradient threshold	1
Critic Regularization Factor	2.5×10^{-4}
Discount Factor	0.99
Experience Buffer Length	2×10^{6}
Mini Batch Size	64
Target Smooth Factor	0.005
Target Update Frequency	2
Clustering DNN learning rate	5×10^{-3}

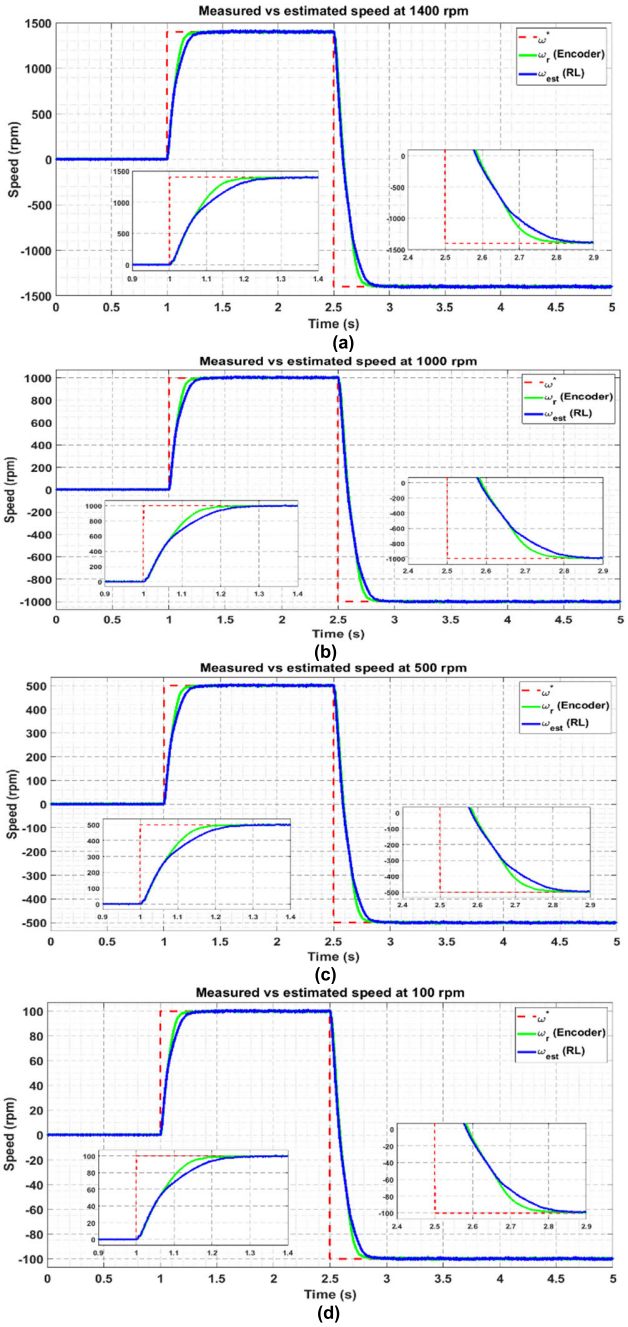

FIGURE 16. Performance comparisons of measured speed (encoder) and estimated speed (RL) with ST-FLC Sim 9-rule at (a) 1400 rpm, (b) 1000 rpm (c) 500 rpm and (d) 100 rpm.

Consistent speed behaviour is maintained at both high and low speeds, showcasing the trained RL policy's accuracy in estimating motor speed. The estimated speed may experience a longer rise time compared to the measured (encoder) speed due to the high penalty terms set during training, which encourages the RL agent to avoid exceeding the rated speed. For safety reasons, the estimated speed with sensorless RL quickly tracks the measured speed and then slows down as it approaches the desired speed to prevent high overshoot and avoid exceeding the rated speed.

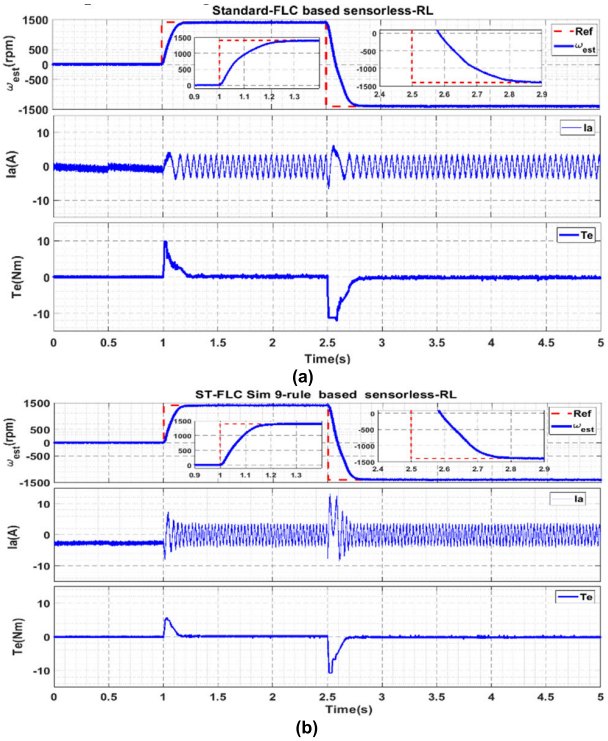

FIGURE 17. Performances of speed, current, and torque with sensorless-RL speed estimation for, (a) 49-rule FLC, and (b) ST-FLC Sim 9-rule.

For the remaining performance tests, sensorless-RL is used for speed estimation and incorporated into the feedback loop, meaning the tests were conducted as sensorless drives without a speed encoder. Performance comparisons of standard FLC 49-rule and proposed ST-FLC Sim 9-rule are conducted based on experimental testing with the estimated speed based on sensorless-RL (ω_est) is used in most of the comparison tests for both controllers. At a rated speed of 1400 rpm with no-load condition, the performances of speed, current and estimated torque for standard FLC 49-rule and proposed ST-FLC Sim 9-rule are presented in Fig.17. The graphs in Fig.17 from top to bottom are the estimated speed based on sensorless-RL, ω_est, phase A stator current,i_a, and estimated torque, T_e. Additionally, the controllers are evaluated at different speeds, including 700,300 and 100 rpm, as depicted in Fig.18.

The proposed ST-FLC Sim 9-rule demonstrated superior performance compared to standard 49-rule FLC at different operating conditions. Faster settling time, low toque and current fluctuations are experienced by the proposed ST-FLC Sim 9-rule at a rated speed of 1400 rpm. Additionally, ST-FLC Sim 9-rule maintained a good performance at lower speed operations (700rpm,300rpm and100rpm) compared to standard FLC 49-rule.

Moreover, the controllers are evaluated against load disturbances by applying a sudden load to the motor shaft. Two load tests are performed: a full load test and a half load test. In the full load test, the motor operates at a steady state of

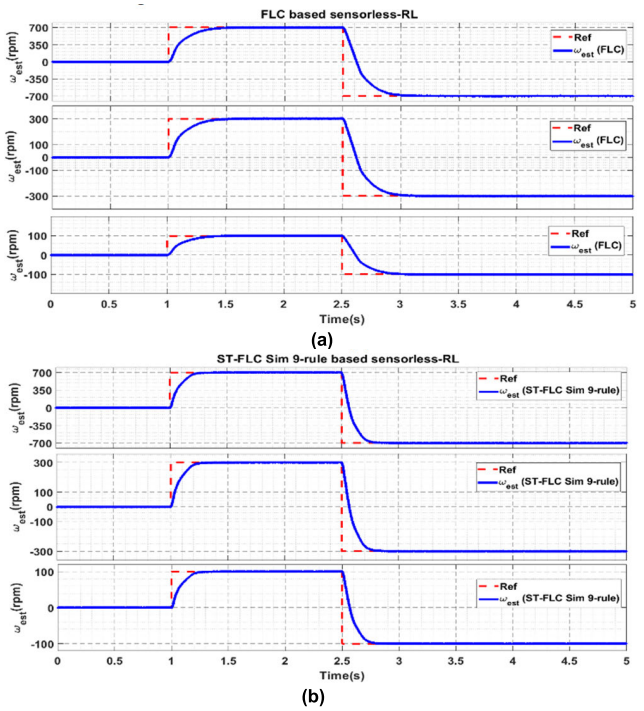

FIGURE 18. Performance of different speed operations with sensorless-RL speed estimation for, (a) 49-rule FLC, and (b) ST-FLC Sim 9-rule.

1400 rpm before a rated torque of 10 Nm is applied to the motor shaft. The response is captured in Fig. 19(a). For the half load test, a torque of 5 Nm is applied, and the response is shown in Fig. 19(b).

The proposed ST-FLC Sim 9-rule demonstrated superior load disturbance rejection capability compared to the standard 49-rule FLC in both tests. During the full load test, the ST-FLC Sim 9-rule experienced a speed drop of 140 rpm with a recovery time of 0.2465 seconds, whereas the standard 49-rule FLC recorded a speed drop of 155 rpm with a recovery time of 0.3562 seconds. In the half load test, the ST-FLC Sim 9-rule had a speed drop of 63.38 rpm and a recovery time of 0.1012 seconds, while the standard 49-rule FLC showed a speed drop of 94.82 rpm with a recovery time of 0.2022 seconds. These results highlight the improved performance of the ST-FLC Sim 9-rule in handling load disturbances. To gain a better understanding of the effectiveness of the proposed ST-FLC Sim 9-rule-based sensorless-RL IM drive, quantitative evaluation and comparison with a standard controller are conducted. The harmonics spectrum of stator current, i_a, was computed for standard FLC and ST-FLC Sim-9-rule as depicted in Fig.20. Low total harmonics distribution (THD) of 5.53% was produced by the proposed ST-FLC Sim 9-rule compared to 6.50% produced by the standard FLC 49-rule. Other transient and steady-state characteristics, including the settling time, overshot, and the steady-state ripples of speed, current and torque, are numerically computed for both controllers as presented in Table 5. Additionally, the numerical values previously obtained in the simulation are added to Table 4 for comparison with

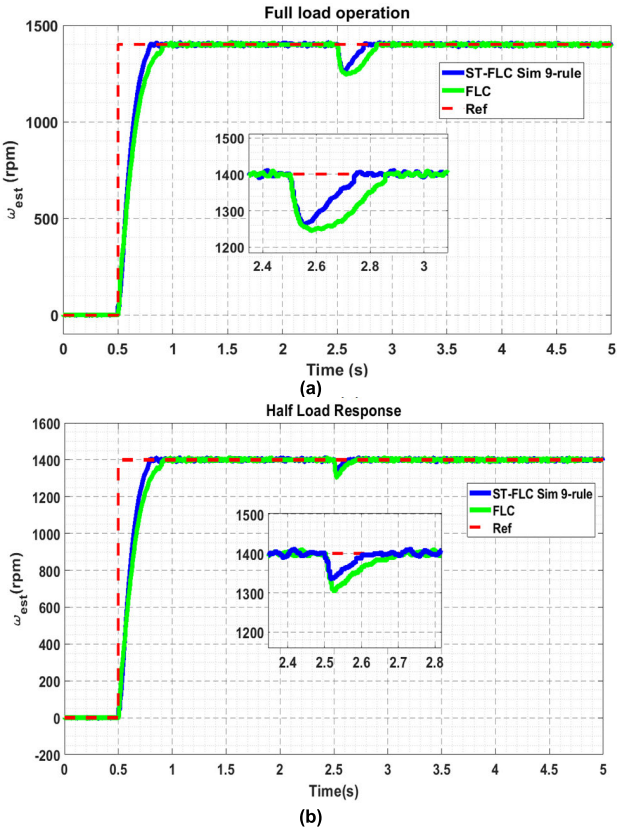

FIGURE 19. Load disturbance comparisons of 49-rule FLC and ST-FLC Sim 9-rule with sensorless-RL speed estimation at 1400rpm for, (a) Full-Load test (10Nm), and (b) Half-Load test (5Nm).

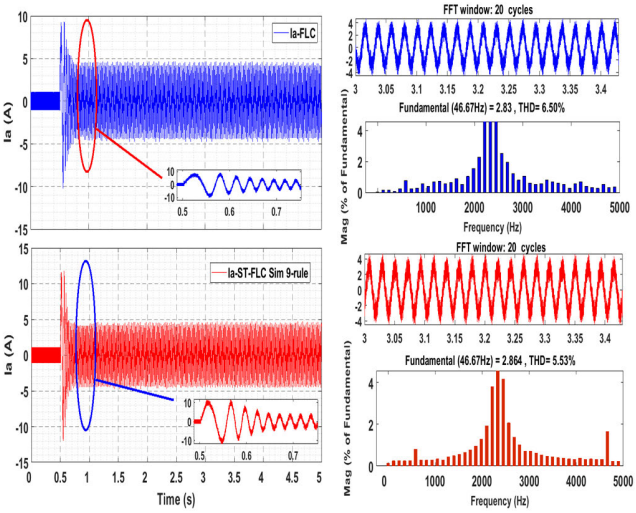

FIGURE 20. THD spectrum comparisons of 49-rule FLC and ST-FLC Sim 9-rule with sensorless-RL speed estimation at 1400rpm.

the experimental values and to show the effectiveness of the proposed method in the real-time application and the advantages of reducing the computation requirement. The proposed ST-FLC Sim-9-rule showed superior experimental performance compared to FLC-49-rules in terms of different

TABLE 6. Simulation and experimental quantitative analysis based on transient and steady-state conditions.

Property / Controller	Test	T_s(s)	OS%	ω_{ripple} (rpm)	$i_{a_{ripple}}$ (A)	T_{ripple} (Nm)
Standard FLC 49-rule.	Sim	0.1164	0.625	0.2847	0.8374	2.1945
	Exp	0.4398	0.6429	0.4592	2.3560	3.2945
ST-FLC Sim 9-rule	Sim	0.1176	0.3895	0.2595	0.8426	2.1925
	Exp	0.2178	0.3478	0.3134	1.8762	2.8013

TABLE 7. Computational time comparison of standard49-rule FLC and ST-FLc sim 9-rule with sensorless-RL speed estimation.

Controller	Computational time
Standard FLC 49-rule	$945\mu s$
ST-FLC Sim 9-rule	$353\mu s$

TABLE 8. IM parameters.

Parameter	Value
Rated frequency	50Hz
Rated voltage	500Vdc
Rated power	2hp
Rated speed	1430 rpm
Rated current	3.58 A
Rated torque	10Nm
Motor efficiency	85%
Number of poles (p)	4
Magnetizing inductance (L_m)	311mH
Rotor inductance(L_s)	325mH
Rotor resistance (R_s)	3.6Ω
Stator inductance(L_r)	320mH
Stator resistance (R_s)	3.4Ω
Inertia (J)	$0.01\ kgm^2$

performance measures. This is attributed to the ability of the proposed method to significantly reduce the computation requirement as demonstrated in Table 6. The proposed method requires approximately a third of the computational time needed for standard FLC-49-rules.

VII. CONCLUSION

This paper proposed an integrated sensorless IM drive with a simplified self-tuning FLC (ST-FLC) and data-driven RL for speed estimation. Conventional sensor-based IM drives with standard FLC may deteriorate the performance due to the sensor measurement error and huge computational requirements associated with a big number of FLC rules. To deal with these issues, the proposed ST-FLC Sim 9-rule based sensorless-RL utilized a simplified 9-rule FLC instead of an intensive 49-rule along with a simple self-tuning mechanism. Furthermore, a computationally efficient sensorless-RL is used to eliminate the encoder measurement error and reduce the overall IM drive cost.

The proposed method offers several advantages over conventional IM drives. By simplifying the FLC rules to a 9-rule set and maintaining adaptability through a simple self-tuning method, the computational burden is significantly reduced. The elimination of the encoder using a computationally efficient RL policy further enhances the system's performance and cost-effectiveness. Unlike most existing ST-FLC methods, the proposed approach uses simple mathematical equations for self-tuning and a pre-trained RL policy for speed estimation, reducing the overall computational resources required. This significant reduction in computational time leads to notable improvements in several experimental performance metrics.

For safety reasons, high penalty terms are set during the training of sensorless-RL to discourage the agent from exceeding the rating speed and increasing the overshot. This explains the slow rise time of the estimated speed as it gets close to the desired speed. In future work, a data-driven RL-based speed controller will be developed to replace the fuzzy-based controller, addressing performance degradation due to changes in operating conditions and variations in machine parameters.

APPENDIX

See the Table 8.

REFERENCES

[1] A. T. de Almeida, F. J. T. E. Ferreira, and G. Baoming, "Beyond induction motors—Technology trends to move up efficiency," in *Proc. 49th IEEE/IAS Ind. Commercial Power Syst. Tech. Conf.*, Apr. 2013, pp. 1–13.
[2] Y. Merizalde, L. Hernández-Callejo, and O. Duque-Perez, "State of the art and trends in the monitoring, detection and diagnosis of failures in electric induction motors," *Energies*, vol. 10, no. 7, p. 1056, Jul. 2017.
[3] N. Farah, M. H. N. Talib, Z. Ibrahim, Q. Abdullah, Ö. Aydoğdu, Z. Rasin, A. Jidin, and J. M. Lazi, "Analysis and investigation of different advanced control strategies for high-performance induction motor drives," *TELKOMNIKA, Telecommun. Comput. Electron. Control*, vol. 18, no. 6, p. 3303, Dec. 2020.
[4] J. Bocker and S. Mathapati, "State of the art of induction motor control," in *Proc. IEEE Int. Electr. Mach. Drives Conf.*, May 2007, pp. 1459–1464.
[5] L. K. Jisha and A. A. Powly Thomas, "A comparative study on scalar and vector control of induction motor drives," in *Proc. Int. Conf. Circuits, Controls Commun. (CCUBE)*, Dec. 2013, pp. 1–5.
[6] A. Smith, S. Gadoue, M. Armstrong, and J. Finch, "Improved method for the scalar control of induction motor drives," *IET Electr. Power Appl.*, vol. 7, no. 6, pp. 487–498, Jul. 2013.
[7] H. Le-Huy, "Comparison of field-oriented control and direct torque control for induction motor drives," in *Proc. Conf. Rec. IEEE Ind. Appl. Conf., 34th IAS Annu. Meeting*, vol. 2, Oct. 1999, pp. 1245–1252.
[8] F. Wang, Z. Zhang, X. Mei, J. Rodríguez, and R. Kennel, "Advanced control strategies of induction machine: Field oriented control, direct torque control and model predictive control," *Energies*, vol. 11, no. 1, p. 120, Jan. 2018.
[9] M. Aktas, K. Awaili, M. Ehsani, and A. Arisoy, "Direct torque control versus indirect field-oriented control of induction motors for electric vehicle applications," *Eng. Sci. Technol., Int. J.*, vol. 23, no. 5, pp. 1134–1143, Oct. 2020.
[10] M. N. Uddin, T. S. Radwan, and M. A. Rahman, "Performances of fuzzy-logic-based indirect vector control for induction motor drive," *IEEE Trans. Ind. Appl.*, vol. 38, no. 5, pp. 1219–1225, Sep. 2002.
[11] D. Casadei, F. Profumo, G. Serra, and A. Tani, "FOC and DTC: Two viable schemes for induction motors torque control," *IEEE Trans. Power Electron.*, vol. 17, no. 5, pp. 779–787, Sep. 2002.
[12] M. Pucci, "Direct field oriented control of linear induction motors," *Electr. Power Syst. Res.*, vol. 89, pp. 11–22, Aug. 2012.
[13] M. Masiala, B. Vafakhah, J. Salmon, and A. M. Knight, "Fuzzy self-tuning speed control of an indirect field-oriented control induction motor drive," *IEEE Trans. Ind. Appl.*, vol. 44, no. 6, pp. 1732–1740, Jul. 2008.

[14] M. H. N. Talib, Z. Ibrahim, N. A. Rahim, and A. S. A. Hasim, "Comparison analysis of indirect FOC induction motor drive using PI, anti-windup and pre filter schemes," *Int. J. Power Electron. Drive Syst. (IJPEDS)*, vol. 5, no. 2, p. 219, Oct. 2014.

[15] Z. Guo, J. Zhang, Z. Sun, and C. Zheng, "Indirect field oriented control of three-phase induction motor based on current-source inverter," *Proc. Eng.*, vol. 174, pp. 588–594, Jan. 2017.

[16] K. Zeb, Z. Ali, K. Saleem, W. Uddin, M. A. Javed, and N. Christofides, "Indirect field-oriented control of induction motor drive based on adaptive fuzzy logic controller," *Electr. Eng.*, vol. 99, no. 3, pp. 803–815, Sep. 2017.

[17] M. H. N. Talib, Z. Ibrahim, and A. S. A. Hasim, "Implementation of anti-windup PI speed controller for induction motor drive using dSPACE and MATLAB/Simulink environment," *Austral. J. Basic Appl. Sci.*, vol. 7, no. 7, pp. 348–357, 2013.

[18] J. M. Lazi, Z. Ibrahim, M. Sulaiman, I. W. Jamaludin, and M. Y. Lada, "Performance comparison of SVPWM and hysteresis current control for dual motor drives," in *Proc. IEEE Appl. Power Electron. Colloq. (IAPEC)*, Apr. 2011, pp. 75–80.

[19] T. Mishra, A. Devanshu, N. Kumar, and A. R. Kulkarni, "Comparative analysis of hysteresis current control and SVPWM on fuzzy logic based vector controlled induction motor drive," in *Proc. IEEE 1st Int. Conf. Power Electron., Intell. Control Energy Syst. (ICPEICES)*, Jul. 2016, pp. 1–6.

[20] R. Arulmozhiyal and K. Baskaran, "Space vector pulse width modulation BasedSpeed control of induction motor using FuzzyPI controller," *Int. J. Comput. Electr. Eng.*, vol. 1, no. 1, p. 98, 2009.

[21] S. M. Tripathi, A. Mishra, and A. K. Pandey, "High performance speed tracking of CSI-fed SCIM drive employing a variable-gain proportional-integral (VGPI) speed controller," *J. Electr. Syst. Inf. Technol.*, vol. 5, no. 3, pp. 635–652, Dec. 2018.

[22] R. Thangaraj, T. R. Chelliah, M. Pant, A. Abraham, and C. Grosan, "Optimal gain tuning of PI speed controller in induction motor drives using particle swarm optimization," *Log. J. IGPL*, vol. 19, no. 2, pp. 343–356, Apr. 2011.

[23] D. Zhang, H. Li, and E. G. Collins, "Digital anti-windup PI controllers for variable-speed motor drives using FPGA and stochastic theory," *IEEE Trans. Power Electron.*, vol. 21, no. 5, pp. 1496–1501, Sep. 2006.

[24] T. Sreekumar and K. S. Jiji, "Comparison of proportional-integral (P–I) and integral-proportional (I–P) controllers for speed control in vector controlled induction motor drive," in *Proc. 2nd Int. Conf. Power, Control Embedded Syst.*, Dec. 2012, pp. 1–6.

[25] M. S. Zaky, "A self-tuning PI controller for the speed control of electrical motor drives," *Electr. Power Syst. Res.*, vol. 119, pp. 293–303, Feb. 2015.

[26] J. Talla, V. Q. Leu, V. Šmídl, and Z. Peroutka, "Adaptive speed control of induction motor drive with inaccurate model," *IEEE Trans. Ind. Electron.*, vol. 65, no. 11, pp. 8532–8542, Nov. 2018.

[27] W.-J. Wang and C.-C. Wang, "A new composite adaptive speed controller for induction motor based on feedback linearization," *IEEE Trans. Energy Convers.*, vol. 13, no. 1, pp. 1–6, Mar. 1998.

[28] W.-J. Wang and C.-C. Wang, "A rotor-flux-observer-based composite adaptive speed controller for an induction motor," *IEEE Trans. Energy Convers.*, vol. 12, no. 4, pp. 323–329, Dec. 1997, doi: 10.1109/60.638868.

[29] F. Lima, W. Kaiser, I. N. da Silva, and A. A. de Oliveira, "Speed neuro-fuzzy estimator applied to sensorless induction motor control," *IEEE Latin Amer. Trans.*, vol. 10, no. 5, pp. 2065–2073, Sep. 2012.

[30] N. Farah, M. Talib, Z. Ibrahim, M. Azri, Z. Rasin, and J. M. Lazi, "Self-tuning fuzzy logic control based on MRAS for induction motor drives," in *Proc. 5th IET Int. Conf. Clean Energy Technol. (CEAT)*, Kuala Lumpur, 2018, pp. 1–6, doi: 10.1049/cp.2018.1351.

[31] S. Mencou, M. B. Yakhlef, and E. B. Tazi, "Fuzzy logic speed controller for robust direct torque control of induction motor drives," in *Digital Technologies and Applications*. Cham, Switzerland: Springer, 2023, pp. 601–611.

[32] Z. Ibrahim and E. Levi, "A comparative analysis of fuzzy logic and PI speed control in high-performance AC drives using experimental approach," *IEEE Trans. Ind. Appl.*, vol. 38, no. 5, pp. 1210–1218, Sep. 2002.

[33] H. AçIKGöZ, O. F. Kececioglu, A. Gani, and M. Sekkeli, "Speed control of direct torque controlled induction motor by using PI, anti-windup PI and fuzzy logic controller," *Int. J. Intell. Syst. Appl. Eng.*, vol. 2, no. 3, p. 58, Oct. 2014.

[34] Y. K. Sahu, K. Quraishi, S. Rajwade, and P. Choudhary, "Comparative analysis of PI & fuzzy logic controller based induction motor drive," in *Proc. Int. Conf. Electr. Power Energy Syst. (ICEPES)*, Dec. 2016, pp. 210–214.

[35] M. J. Patyra, J. L. Grantner, and K. Koster, "Digital fuzzy logic controller: Design and implementation," *IEEE Trans. Fuzzy Syst.*, vol. 4, no. 4, pp. 439–459, Nov. 1996, doi: 10.1109/91.544304.

[36] İ. Eker and Y. Torun, "Fuzzy logic control to be conventional method," *Energy Convers. Manage.*, vol. 47, no. 4, pp. 377–394, Mar. 2006.

[37] N. Farah, M. H. N. Talib, Z. Ibrahim, Q. Abdullah, Ö. Aydogdu, M. Azri, J. B. M. Lazi, and Z. M. Isa, "Investigation of the computational burden effects of self-tuning fuzzy logic speed controller of induction motor drives with different rules sizes," *IEEE Access*, vol. 9, pp. 155443–155456, 2021.

[38] N. Farah, M. H. N. Talib, Z. Ibrahim, M. Azri, and Z. Rasin, "Self-tuned output scaling factor of fuzzy logic speed control of induction motor drive," in *Proc. 7th IEEE Int. Conf. Syst. Eng. Technol. (ICSET)*, Oct. 2017, pp. 134–139.

[39] R. K. Mudi and N. R. Pal, "A robust self-tuning scheme for PI- and PD-type fuzzy controllers," *IEEE Trans. Fuzzy Syst.*, vol. 7, no. 1, pp. 2–16, Feb. 1999, doi: 10.1109/91.746295.

[40] N. Farah, M. H. N. Talib, N. S. M. Shah, Q. Abdullah, Z. Ibrahim, J. B. M. Lazi, and A. Jidin, "A novel self-tuning fuzzy logic controller based induction motor drive system: An experimental approach," *IEEE Access*, vol. 7, pp. 68172–68184, 2019.

[41] M. H. N. Talib, Z. Ibrahim, N. Abd. Rahim, R. Zulhani, N. Nordin, N. Farah, and A. M. Razali, "An improved simplified rules fuzzy logic speed controller method applied for induction motor drive," *ISA Trans.*, vol. 105, pp. 230–239, Oct. 2020.

[42] Q. A. Tarbosh, Ö. Aydogdu, N. Farah, M. H. N. Talib, A. Salh, N. Çankaya, F. A. Omar, and A. Durdu, "Review and investigation of simplified rules fuzzy logic speed controller of high performance induction motor drives," *IEEE Access*, vol. 8, pp. 49377–49394, 2020.

[43] M. H. N. Talib, Z. Ibrahim, Z. Rasin, J. M. Lazi, and S. N. M. Isa, "Simplified self-tuning fuzzy logic speed controller for induction motor drive," in *Proc. IEEE Int. Conf. Power Energy (PECon)*, Nov. 2016, pp. 188–193.

[44] M. Z. Ismail, M. H. N. Talib, Z. Ibrahim, J. Mat Lazi, and Z. Rasin, "Experimental simplified rule of self tuning fuzzy logic-model reference adaptive speed controller for induction motor drive," *Indonesian J. Electr. Eng. Comput. Sci.*, vol. 20, no. 3, p. 1653, Dec. 2020.

[45] I. I. Incze, C. Szabó, and M. Imecs, "Incremental encoder in electrical drives: Modeling and simulation," in *Computational Intelligence in Engineering* (Studies in Computational Intelligence), vol. 313. Berlin, Germany: Springer, 2010, pp. 287–300.

[46] J. M. Aller, T. G. Habetler, R. G. Harley, R. M. Tallam, and S. B. Lee, "Sensorless speed measurement of AC machines using analytic wavelet transform," *IEEE Trans. Ind. Appl.*, vol. 38, no. 5, pp. 1344–1350, Sep. 2002.

[47] F. Alonge, F. D'Ippolito, and A. Sferlazza, "Sensorless control of induction-motor drive based on robust Kalman filter and adaptive speed estimation," *IEEE Trans. Ind. Electron.*, vol. 61, no. 3, pp. 1444–1453, Mar. 2014.

[48] M. S. Zaky, M. K. Metwaly, H. Z. Azazi, and S. A. Deraz, "A new adaptive SMO for speed estimation of sensorless induction motor drives at zero and very low frequencies," *IEEE Trans. Ind. Electron.*, vol. 65, no. 9, pp. 6901–6911, Sep. 2018.

[49] Z. Aydogmus and O. Aydogmus, "A comparison of artificial neural network and extended Kalman filter based sensorless speed estimation," *Measurement*, vol. 63, pp. 152–158, Mar. 2015.

[50] E. Zerdali, "Adaptive extended Kalman filter for speed-sensorless control of induction motors," *IEEE Trans. Energy Convers.*, vol. 34, no. 2, pp. 789–800, Jun. 2019.

[51] M. Jouili, K. Jarray, Y. Koubaa, and M. Boussak, "Luenberger state observer for speed sensorless ISFOC induction motor drives," *Electr. Power Syst. Res.*, vol. 89, pp. 139–147, Aug. 2012.

[52] A. Derdiyok, M. K. Guven, H. Rehman, N. Inanc, and L. Xu, "Design and implementation of a new sliding-mode observer for speed-sensorless control of induction machine," *IEEE Trans. Ind. Electron.*, vol. 49, no. 5, pp. 1177–1182, Oct. 2002.

[53] K.-B. Lee and F. Blaabjerg, "Improved sensorless vector control for induction motor drives fed by a matrix converter using nonlinear modeling and disturbance observer," *IEEE Trans. Energy Convers.*, vol. 21, no. 1, pp. 52–59, Mar. 2006.

[54] M. Korzonek, G. Tarchala, and T. Orlowska-Kowalska, "A review on MRAS-type speed estimators for reliable and efficient induction motor drives," *ISA Trans.*, vol. 93, pp. 1–13, Oct. 2019.
[55] K. Ide, J.-I. Ha, and M. Sawamura, "A hybrid speed estimator of flux observer for induction motor drives," *IEEE Trans. Ind. Electron.*, vol. 53, no. 1, pp. 130–137, Feb. 2006.
[56] C.-M. Lee and C.-L. Chen, "Observer-based speed estimation method for sensorless vector control of induction motors," *IEE Proc.-Control Theory Appl.*, vol. 145, no. 3, pp. 359–363, May 1998.
[57] C.-H.-T. H.-C. Lu, "Observer-based speed estimation method for sensorless vector control using artificial neural network," *Electr. Mach. Power Syst.*, vol. 28, no. 9, pp. 861–873, Sep. 2000.
[58] S. Maiti, V. Verma, C. Chakraborty, and Y. Hori, "An adaptive speed sensorless induction motor drive with artificial neural network for stability enhancement," *IEEE Trans. Ind. Informat.*, vol. 8, no. 4, pp. 757–766, Nov. 2012.
[59] A. Accetta, M. Cirrincione, M. Pucci, and G. Vitale, "Neural sensorless control of linear induction motors by a full-order Luenberger observer considering the end effects," *IEEE Trans. Ind. Appl.*, vol. 50, no. 3, pp. 1891–1904, May 2014.
[60] A. Kushwaha and M. Gopal, "Reinforcement learning-based controller for field-oriented control of induction machine," in *Soft Computing for Problem Solving*, J. C. Bansal, K. N. Das, A. Nagar, K. Deep, and A. K. Ojha, Eds., Singapore: Springer, 2019, pp. 737–749.
[61] X. Qi, W. Cao, and L. Aarniovuori, "Reinforcement learning based parameter lookup table generating method for optimal torque control of induction motors," *IEEE Trans. Ind. Electron.*, vol. 70, no. 5, pp. 4516–4525, May 2023.
[62] P. Saurabh, N. Nagabhooshanam, D. S. Kumar, A. C. S. Akula, G. V. Londhe, V. S. Rao, and V. U. P. Lavanya, "Enhanced induction motor control using deep reinforcement learning and PWM with DTC," *Electr. Power Compon. Syst.*, vol. 2023, pp. 1–13, Nov. 2023.
[63] N. Farah, G. Lei, J. Zhu, and Y. Guo, "Robust model-free reinforcement learning based current control of PMSM drives," *IEEE Trans. Transport. Electrific.*, 2024, doi: 10.1109/tte.2024.3400534.
[64] M. Nicola, C.-I. Nicola, C. Ionete, D. Şendrescu, and M. Roman, "Improved performance for PMSM sensorless control based on robust-type controller, ESO-type observer, multiple neural networks, and RL-TD3 agent," *Sensors*, vol. 23, no. 13, p. 5799, Jun. 2023.
[65] M. Nicola, C.-I. Nicola, C. Constantinescu, and R. Prejbeanu, "Improvement performances of the SMO observer for PMSM sensorless control based on DTC strategy using simulated annealing and reinforcement learning TD3 agent," *Syst. Theory, Control Comput. J.*, vol. 3, no. 2, pp. 36–43, Dec. 2023.
[66] A. Mustafa, T. Sasamura, and T. Morita, "Sensorless speed control of ultrasonic motors using deep reinforcement learning," *IEEE Sensors J.*, vol. 24, no. 3, pp. 4023–4035, Feb. 2024.
[67] W. Zhifu, F. Jun, S. Zhijian, and S. Qiang, "Study on speed sensor-less vector control of induction motors based on AMEsim-MATLAB/Simulink simulation," *Energy Proc.*, vol. 105, pp. 2378–2383, May 2017.
[68] A. Pal, R. Kumar, and S. Das, "Sensorless speed control of induction motor driven electric vehicle using model reference adaptive controller," *Energy Proc.*, vol. 90, pp. 540–551, Dec. 2016.
[69] D. Bao, H. Wang, X. Wang, and C. Zhang, "Sensorless speed control based on the improved Q-MRAS method for induction motor drives," *Energies*, vol. 11, no. 1, p. 235, Jan. 2018.
[70] N. Kobayashi, K. Kondo, and O. Yamazaki, "Induction motor speed sensor-less vector control with the mechanical simulator with disturbance torque compensation," in *Proc. Int. Symp. Power Electron., Electr. Drives, Autom. Motion*, Jun. 2014, pp. 1160–1165.
[71] S. Chekroun, M. Zerikat, A. Mechernene, and N. Benharir, "Novel observer scheme of fuzzy-MRAS sensorless speed control of induction motor drive," *J. Phys., Conf. Ser.*, vol. 783, Jan. 2017, Art. no. 012045.
[72] K. Bhuvaneshvari and M. G. Mahendran, "PI and fuzzy based sensorless speed control of induction motor," *IOSR J. Electr. Electron. Eng.*, vol. 9, no. 2, pp. 41–46, 2014.
[73] A. Kumar and T. Ramesh, "MRAS speed estimator for speed sensorless IFOC of an induction motor drive using fuzzy logic controller," in *Proc. Int. Conf. Energy, Power Environ., Towards Sustain. Growth (ICEPE)*, Jun. 2015, pp. 1–6.
[74] K. Kouzi and M. Saïd Naït-Saïd, "Adaptive fuzzy logic speed-sensorless control improvement of induction motor for standstill and low speed operations," *COMPEL-Int. J. Comput. Math. Electr. Electron. Eng.*, vol. 26, no. 1, pp. 22–35, Jan. 2007.
[75] N. Farah, M. H. N. Talib, Z. B. Ibrahim, Q. Abdullah, Ö. Aydoğdu, J. M. Lazi, and Z. Isa, "Fuzzy membership functions tuning for speed controller of induction motor drive: Performance improvement," *Indonesian J. Electr. Eng. Comput. Sci.*, vol. 23, no. 3, p. 1258, Sep. 2021.
[76] N. Farah, M. Talib, Z. Ibrahim, Z. Rasin, and Z. Rizman, "Experimental investigation of different rules size of fuzzy logic controller for vector control of induction motor drives," *J. Fundam. Appl. Sci.*, vol. 10, no. 6S, pp. 1696–1717, 2018.
[77] D. K. Sambariya and R. Prasad, "A novel fuzzy rule matrix design for fuzzy logic-based power system stabilizer," *Electr. Power Compon. Syst.*, vol. 45, no. 1, pp. 34–48, Jan. 2017.

QAZWAN ABDULLAH (Senior Member, IEEE) was born in Taiz, Yemen. He received the bachelor's and M.Sc. degrees in electrical and electronic engineering from Universiti Tun Hussein Onn Malaysia (UTHM), in 2013 and 2015, respectively. Currently, he is a Research Assistant at UTHM. He has more than 40 scientific publications. His research interests include control theory, adaptive fuzzy logic controllers, mobile communications (5G/6G), fuzzy logic control and its applications, motor drive, electric vehicles, and antenna filter design.

NABIL FARAH (Graduate Student Member, IEEE) received the bachelor's and master's degrees in electrical engineering from Universiti Teknikal Malaysia Melaka, in 2015 and 2018, respectively, and the Ph.D. degree in electrical engineering from the University of Technology Sydney (UTS), in 2024. He is currently a Research Associate at UTS and a Lecturer at Melbourne Institute of Technology (MIT), Sydney. His research interests include electrical machine drive control and optimization, predictive control, and machine learning methods for PMSM drives.

MUSTAFA SAMI AHMED (Student Member, IEEE) received the B.S. degree in computer communication engineering from the Al Rafidain University College, Baghdad, Iraq, in 2011, the M.S. degree in engineering from the Faculty of Electrical and Electronic Engineering, University Tun Hussein Onn Malaysia, Johor, Malaysia, in 2015, and the Ph.D. degree in communication engineering from University Tun Hussein Onn Malaysia, in 2020. He is currently a Lecturer with the Department of Communication Engineering, University of Technology-Iraq. His research interests include underwater acoustic communication, digital signal processing, and wireless communication.

NOR SHAHIDA MOHD SHAH (Senior Member, IEEE) received the B.Eng. degree in electrical and electronic engineering from Tokyo Institute of Technology, Japan, in 2000, the M.Sc. degree in optical communication from the University of Malaya, Malaysia, in 2003, and the Ph.D. degree in electrical, electronics and system engineering from Osaka University, Japan, in 2012. She is currently a Senior Lecturer at Universiti Tun Hussein Onn Malaysia. Her research interests include optical and wireless communication.

ÖMER AYDOĞDU (Member, IEEE) was born in Konya, Türkiye, in 1973. He received the B.S., M.S., and Ph.D. degrees in electrical and electronics engineering from Selçuk University, Konya, in 1995, 1999, and 2006, respectively. From 1996 to 2007, he was a Research Assistant with the Department of Electrical and Electronics Engineering, Selçuk University. From 2007 to 2018, he was an Assistant Professor and an Associate Professor with the Department of Electrical and Electronics Engineering, Selçuk University. From 2018 to 2020, he was an Associate Professor with the Department of Electrical and Electronics Engineering, Konya Technical University, Konya, where he has been a Professor, since 2020. He is the author of a book chapter and more than 70 scientific publications. His research interests include control theory, adaptive control systems, fractional order control, fuzzy logic control and applications, and brushless dc motors and drives.

MD HAIRUL NIZAM TALIB (Member, IEEE) was born in Malaysia, in 1976. He received the B.S. degree in electrical engineering from Universiti Teknologi Malaysia (UTM), Johor, Malaysia, in 1999, the M.S. degree in electrical engineering from the University of Nottingham, Nottingham, U.K., in 2005, and the Ph.D. degree from Universiti Teknikal Malaysia Melaka (UTeM), Malaysia, in 2016. He is currently a Senior Lecturer at UTeM. His main research interests include power electronics, fuzzy logic control, and motor drives.

YAHYA M. AL-MOLIKI received the B.Sc. degree in electrical engineering from Sana'a University, Sana'a, Yemen, in 2007, the M.Sc. degree (Hons.) in engineering from the University of Malaya, Malaysia, in 2012, and the Ph.D. degree in electrical engineering from King Saud University, Riyadh, Saudi Arabia, in 2019. His research interests include physical-layer security for indoor VLC networks and OFDM-based optical systems.

ABBAS UĞURENVER was born in Mosul, Iraq. He received the B.S. degree in electrical power engineering technology from Northern Technical University, Iraq, in 2010, the M.S. degree in electronics and communication engineering from Çankaya University, Türkiye, in 2012, and the Ph.D. degree in electrical and electronics engineering from the Faculty of Engineering and Natural Sciences, Konya Technical University, Konya, Türkiye, in 2020. He is currently an Assistant Professor with the Department of Electrical and Electronic Engineering, Istanbul Aydin University.

MOHAMMED A. A. AL-MEKHALFI was born in Edinburgh, Scotland, U.K., in 1990. He received the B.S. degree in electrical engineering (mechatronics) and the M.Eng. degree in electrical engineering (mechatronics and automatic control) from the Faculty of Electrical Engineering, Universiti Teknologi Malaysia (UTM), Malaysia, in 2015 and 2017, respectively. His research interests include control, autonomous mobile robots, and artificial intelligence.

MUHAMMAD ZAID AIHSAN (Student Member, IEEE) was born in Penang, Malaysia. He received the Diploma degree in mechatronic engineering from Japan-Malaysia Technical Institute (JMTi) in 2010, the B.Eng. degree in industrial electronic and the M.Sc. degree in electrical system from University Malaysia Perlis (UniMAP), Perlis, Malaysia, in 2013 and 2016, respectively, and the Ph.D. degree in the field of power electronics and drives from Universiti Teknikal Malaysia Melaka (UTeM), Malaysia, in 2024.

He is currently a Senior Lecturer at the Faculty of Electrical Engineering and Technology, UniMAP. His research interests include the power electronics, motor drive systems, and renewable energy system.

ADEB SALH received the bachelor's degree in electrical and electronic engineering from IBB University, Yemen, in 2007, and the master's and Ph.D. degrees in electrical and electronic engineering from Universiti Tun Hussein Onn Malaysia (UTHM), in 2015 and 2020, respectively. From 2007 to 2012, he was a Lecturer Assistant with the Yareem Community College. From 2020 to 2023, he was a Postdoctoral Researcher with UTHM and UTM, respectively. Currently, he is an Assistant Professor with the Faculty of Information and Communication Technology, Universiti Tunku Abdul Rahman. His research interests include 5G and 6G wireless communications, massive MIMO, artificial intelligence (AI), and the Internet of Things (IoT).